# Angoricity and compactivity describe the jamming transition in soft particulate matter

Kun Wang<sup>1</sup>, Chaoming Song<sup>2</sup>, Ping Wang<sup>3</sup>, Hernán A. Makse<sup>1</sup>

<sup>1</sup>Levich Institute and Physics Department,

City College of New York, New York, NY 10031, US

<sup>2</sup>Center for Complex Network Research,

Department of Physics, Biology and Computer Science,

Northeastern University, Boston, MA 02115, US

<sup>3</sup>FAS Center for Systems Biology, Harvard University, Cambridge, MA 02138, US

(Dated: March 23, 2021)

## Abstract

The application of concepts from equilibrium statistical mechanics to out-of-equilibrium systems has a long history of describing diverse systems ranging from glasses to granular materials. For dissipative jammed systems—particulate grains or droplets—a key concept is to replace the energy ensemble describing conservative systems by the volume-stress ensemble. Here, we test the applicability of the volume-stress ensemble to describe the jamming transition by comparing the jammed configurations obtained by dynamics with those averaged over the ensemble as a probe of ergodicity. Agreement between both methods suggests the idea of "thermalization" at a given angoricity and compactivity. We elucidate the thermodynamic order of the jamming transition by showing the absence of critical fluctuations in static observables like pressure and volume. The approach allows to calculate observables such as the entropy, volume, pressure, coordination number and distribution of forces to characterize the scaling laws near the jamming transition from a statistical mechanics viewpoint.

A granular system compresses into a mechanically stable configuration at a nonzero pressure in response to the application of an external strain [1–3]. This process is typically referred to as the jamming transition and occurs at a critical volume fraction  $\phi_c$  [3]. The application of a subsequent external pressure with the concomitant particle rearrangements and compression results in a set of configurations characterized by the system volume  $V = NV_g/\phi$  ( $\phi$  is the volume fraction of N particles of volume  $V_g$ ) and applied external stress or pressure p (for simplicity we assume isotropic states). It has been long argued whether the jamming transition is a first-order transition at the discontinuity in the average coordination number,  $\langle Z \rangle$ , or a second-order transition with the power-law scaling of the system's pressure as the system approaches jamming with  $\phi - \phi_c \rightarrow 0^+$  [4–7]. Previous work [8–10] has proposed to explain the jamming transition by a field theory in the pressure ensemble. Here, we use the idea of "thermalization" of an ensemble of mechanically stable granular materials at a given volume and pressure to study the jamming transition from a thermodynamic viewpoint.

For a fixed number of grains, there exist many jammed states [11] confined by the external pressure p in a volume V. In an effort to describe the nature of this nonequilibrium system from a statistical mechanics perspective, a pressure-volume ensemble [8, 12–15] was introduced for jammed matter. In the canonical the probability of a state is given by  $\exp[-\mathcal{W}(\partial S/\partial V) - \Gamma(\partial S/\partial \Gamma)]$ , where S is the entropy of the system,  $\mathcal{W}$  is the volume function measuring the volume of the system as a function of the particle coordinates and  $\Gamma \equiv pV$  is the boundary stress (or internal virial) [9] of the system. Just as  $\partial E/\partial S = T$  is the temperature in equilibrium system, the temperature-like variables in jammed systems are the compactivity  $X = \partial V/\partial S$  [12] and the angoricity  $A = \partial \Gamma/\partial S$  [13].

In a recent paper [16] the compactivity was used to describe frictional hard spheres in the volume ensemble. Here, we test the validity of the statistical approach in the combined pressure-volume ensemble to describe deformable, frictionless particles, such as emulsion systems jammed under osmotic pressure near the jamming transition [17]. We demonstrate that the jamming transition can be probed thermodynamically by the angoricity A and the compactivity X. The calculation of jamming "heat" capacities characterizes the system fluctuations and shows the lack of critical fluctuations in the static quantities as the jamming transition point is approached from above  $\phi \to \phi_c^+$ . Thus, the thermodynamical viewpoint determines the order of the phase transition and allows one to calculate the physical observables near jamming.

## I. RESULTS

In general, if the density of states  $g(\Gamma, \phi)$  in the space of jammed configurations (defined as the probability of finding a jammed state at a given  $(\Gamma, \phi)$  at  $A = \infty$ ) is known, then calculations of macroscopic observables, like pressure p and average coordination number Z as a function of  $\phi$ , can be performed by the canonical ensemble average [9, 10] at a given volume:

$$\langle p(\alpha, \phi) \rangle_{\text{ens}} = \frac{1}{\mathcal{Z}} \int_0^\infty p \ g(\Gamma, \phi) \ e^{-\alpha \Gamma} \ d\Gamma,$$
 (1)

and

$$\langle Z(\alpha, \phi) \rangle_{\text{ens}} = \frac{1}{\mathcal{Z}} \int_0^\infty Z \ g(\Gamma, \phi) \ e^{-\alpha \Gamma} \ d\Gamma,$$
 (2)

where the canonical partition function is  $\mathcal{Z} = \int_0^\infty g(\Gamma,\phi) e^{-\alpha\Gamma} d\Gamma$  and the density of states is normalized as  $\int_0^\infty g(\Gamma,\phi) d\Gamma = 1$ . The inverse angoricity is defined as  $\alpha \equiv 1/A = \partial S/\partial\Gamma$ .

At the jamming transition the system reaches isostatic equilibrium, such that the stresses are exactly balanced in the resulting configuration, and there exists a unique solution to the interparticle force equations satisfying mechanical equilibrium. It is well known that observables present power-law scaling [4, 5, 7]:

$$\langle p \rangle_{\rm dyn} \sim (\phi - \phi_c)^a, \qquad \langle Z \rangle_{\rm dyn} - Z_c \sim (\phi - \phi_c)^b,$$
 (3)

where a=3/2 and b=1/2 for Hertzian spheres and  $Z_c=6$  is the coordination number at the isostatic point (J-point) [4]. The average  $\langle \cdots \rangle_{\rm dyn}$  indicates that these quantities are obtained by averaging over packings generated dynamically in either simulations or experiments as opposed to the ensemble average over configurations  $\langle \cdots \rangle_{\rm ens}$  of Eqs. (1)–(2). Comparing the ensemble calculations, Eq. (1)–(2), with the direct dynamical measurements, Eq. (3), provides a basic test of the ergodic hypothesis for the statistical ensemble.

Our approach is the following: We first perform an exhaustive enumeration of configurations to calculate  $g(\Gamma, \phi)$  and obtain  $\langle p(\alpha, \phi) \rangle_{\text{ens}}$  as a function of  $\alpha$  for a given  $\phi$  using Eq. (1). Then, we obtain the angoricity by comparing the pressure in the ensemble average with the one obtained following the dynamical evolution with Molecular Dynamics (MD) simulations. By setting  $\langle p(\alpha, \phi) \rangle_{\text{ens}} = \langle p \rangle_{\text{dyn}}$ , we obtain the angoricity as a function of  $\phi$ . By virtue of obtaining  $\alpha(\phi)$ , all the other observables can be calculated in the ensemble formulation. The ultimate test of ergodicity is realized by comparing the remaining ensemble observables with the corresponding direct dynamical measures. Ensemble calculations.— The density of jammed states  $g(\Gamma, \phi)$  is calculated in the framework of the potential energy landscape (PEL) formulation introduced by Goldstein [18] and Stillinger-Weber [19, 20] to describe supercooled liquids. In the case of frictionless jammed systems, the mechanically stable configurations are defined as the local minima of the potential energy surface (PES) of the system [4, 11] (see Fig. 1 inset for a schematic representation). In the simulations, two spherical soft particles in contact interact via a normal Hertz force [6, 21],  $F_n \propto (\delta r)^{\delta}$ , where  $\delta r$  is the normal overlap between the spheres under deformation and  $\delta = 1.5$ , in a periodically repeated cube [the interparticle potential energy is  $E \propto (\delta r)^{\delta+1}$ , see Materials and Methods Section III A]. The Hertz potential is chosen for its general applicability to granular materials. The results are expected to be independent of the form of the potential. Details of the algorithms [22, 23] to find the local minima of the PES (zero-order saddles) are in the Materials and Methods Section III B. Figure 1 shows  $g(\Gamma, \phi)$  versus  $\Gamma$  for different volume fractions.

**MD calculations.**— The pressure  $\langle p \rangle_{\rm dyn}$  as a function of  $\phi$  is calculated by performing MD simulations. Packings are prepared by compressing a gas of particles from an initial (unjammed) low volume fraction to a final jammed state. This procedure simulates a dynamical packing preparation [24]; details appear in Materials and Methods Section III C. We obtain (Fig. 2A)

$$\langle p \rangle_{\rm dyn} = p_0 \ (\phi - \phi_c)^{1.65} \ , \tag{4}$$

where  $\phi_c = 0.6077$  is the volume fraction corresponding to the isostatic point J [4] following Eq. (3) and  $p_0 = 10.8$ MPa. This critical value and the exponent, a = 1.65, are slightly different than the values obtained for larger systems  $(a = \delta)[4]$ . However, our purpose is to use the same system in the dynamical calculation and the exact enumeration for a proper comparison.

Calculation of angoricity.— For each  $\phi$  we use  $g(\Gamma, \phi)$  to calculate  $\langle p(\alpha) \rangle_{\text{ens}}$  by Eq. (1). Then, we obtain  $\alpha(\phi)$  by setting  $\langle p(\alpha, \phi) \rangle_{\text{ens}} = \langle p \rangle_{\text{dyn}}$  for every  $\phi$  (see Figs. 9 and 10 and Materials and Methods Section III D). The resulting equation of state  $\alpha(\phi)$  is plotted in Fig. 2B and shows that the angoricity follows a power-law, near  $\phi_c$ , of the form:

$$A \propto (\phi - \phi_c)^{\gamma},\tag{5}$$

where the angoricity exponent is  $\gamma = 2.5$ . The result is consistent with  $\gamma = \delta + 1.0$ , suggesting that  $A \propto \Gamma \propto F_n r$ . Angoricity is a measure of the number of ways the stress

can be distributed in a given volume. Since the stresses have a unique solution for a given configuration at the isostatic point,  $\phi_c$ , the corresponding angoricity vanishes. At higher pressure, the system is determined by multiple degrees of freedom satisfying mechanical equilibrium, leading to a higher stress temperature, A. The angoricity can also be viewed as a scale of stability for the system at different volume fractions. Systems jammed at larger volume fractions require higher angoricity (higher driving force) to rearrange.

Test of ergodicity.—In principle, using the inverse angoricity,  $\alpha$ , from Eq. (5) we can calculate any macroscopic statistical observable  $\langle B \rangle_{\text{ens}}$  at a given volume by performing the ensemble average [10]:

$$\langle B(\phi) \rangle_{\text{ens}} = \frac{1}{\mathcal{Z}} \int_0^\infty B \ g(\Gamma, \phi) \ e^{-\alpha \Gamma} \ d\Gamma.$$
 (6)

We test the ergodic hypothesis in the Edwards's ensemble by comparing Eq. (6) with the corresponding value obtained with MD simulations averaged over (250) sample packings,  $B_i$ , generated dynamically:

$$\langle B(\phi) \rangle_{\text{dyn}} = \frac{1}{250} \sum_{i=1}^{250} B_i.$$
 (7)

The comparison is realized by measuring the average coordination number,  $\langle Z \rangle$ , the average force and the distribution of interparticle forces. We calculate  $\langle Z \rangle_{\rm ens}$  by Eq. (2) and  $\langle Z \rangle_{\rm dyn}$  as in Eq. (7). Figures 3A and 3B show that the two independent estimations of the coordination number agree very well:  $\langle Z \rangle_{\rm ens} = \langle Z \rangle_{\rm dyn}$ .

We calculate the ensemble average force  $\langle \overline{F} \rangle_{\rm ens}$  and the average over all the MD packings,  $\langle \overline{F} \rangle_{\rm dyn}$  and find that they coincide very closely (see Fig. 3C). The full distribution of inter-particle forces for jammed systems is also an important observable which has been extensively studied in previous works [4, 25, 26]. The force distribution is calculated in the ensemble  $P_{\rm ens}(F/\overline{F})$  by averaging the force distribution for every configuration in the PES (see Materials and Methods Section III D). Figure 3D shows the distribution functions. The peak of the distribution shown in Fig. 3D indicates that the systems are jammed [4, 25, 26]. Besides the exact shape of the distribution, the similarity between the ensemble and the dynamical calculations shown in Fig. 3D is significant. The study of  $\langle Z \rangle$ ,  $\langle \overline{F} \rangle$  and  $P(F/\overline{F})$  reveals that the statistical ensemble can predict the macroscopic observables obtained in MD. This suggests that the idea of "thermalization" at an angoricity is able to describe the jamming system very well.

Thermodynamic analysis of the jamming transition.— So far we have considered how the angoricity determines the pressure fluctuations in a jammed packing at a fixed  $\phi$ . The role of the compactivity in the jamming transition can be analyzed in terms of the entropy which is easily calculated in the microcanonical ensemble from the density of states. Figure 4 shows  $S = \ln(\Omega(p, \phi))$  ( $\Omega$  is the number of states which is the unnormalized version of  $g(\Gamma, \phi)$ ), which is the non-equilibrium entropy of the system at the given  $(p, \phi)$  in phase space.

We analyze the non-equilibrium entropy surface  $S(\ln(\phi - \phi_c), \ln p)$  plotted versus  $(\ln(\phi - \phi_c), \ln p)$  in Fig. 4 and demonstrate that the MD curve  $\langle p(\phi) \rangle_{\text{dyn}}$  passes along the maximum of the entropy surface constrained by the coupling between p and  $\phi$ , Eq. (3). Thus the points along the entropy surface defined by  $\langle p(\phi) \rangle$  correspond to the equilibrium entropy; such a curve is superimposed to the entropy surface in Fig. 4. Due to the coupling through the contact force law, the maximization of entropy is not on p or  $\phi$  alone but on a combination of both. The entropy S reaches a maximum at the point  $S(\ln(\langle \phi \rangle_{\text{dyn}} - \phi_c), \ln \langle p \rangle_{\text{dyn}})$  when we move along the direction perpendicular to the jamming curve  $\langle p(\phi) \rangle_{\text{dyn}}$  (see the maximization direction in Fig. 4). This is a direct verification of the second-law of thermodynamics: the dynamical measures maximize the entropy of the system.

We can use this result to obtain a relation between angoricity and compactivity. We write  $\ln p = \ln p_0 + a \ln(\phi - \phi_c)$  where a is the exponent in Eq. (3), such that  $S(\ln(\phi - \phi_c), \ln p)$  is maximized at the MD measures according to the direction of  $(-\sin\theta, \cos\theta)$   $(\tan\theta = a$  is the slope of the power-law curve in the  $\log - \log$  plot in Fig. 4). Therefore, neither A nor X can play the role of the temperature of the system alone, but a combination of both determined by entropy maximization satisfying the coupling between stress and strain. Since  $\delta S = 0$  at  $(\ln(\langle \phi \rangle_{\rm dyn} - \phi_c), \ln \langle p \rangle_{\rm dyn})$  along  $(-\sin\theta, \cos\theta)$  then  $(\partial S/\partial \ln p) \cos\theta - (\partial S/\partial \ln(\phi - \phi_c)) \sin\theta = 0$ . We obtain  $c_1\alpha + ac_2\beta = 0$  (where  $c_1 = \Gamma$  and  $c_2 = (\phi - \phi_c)(NV_g/\phi^2)$ ) and the relation between A and X (see Fig. 13 and Materials and Methods Section III E):

$$X = -aA(\phi - \phi_c)/p\phi. \tag{8}$$

From Eq. (8) we obtain that:  $X \propto -(\phi - \phi_c)^{1+a-\gamma}/\phi$  and near  $\phi_c$ :

$$X \sim -(\phi - \phi_c)^2. \tag{9}$$

We notice that the compactivity is negative near the jamming transition. A negative tem-

perature is a general property of systems with bounded energy like spins [27]: the system attains the larger volume (or magnetization in spins) at  $\phi_c$  when  $X \to 0^-$  and not  $X \to +\infty$  [The bounds  $\phi_c \leq \phi \leq 1$  imply that the jamming point at  $X \to 0^-$  is "hotter" than  $X \to +\infty$ . At the same time  $A \to 0^+$  since the pressure vanishes].

We conclude that, A and X alone cannot play the role of temperature. Instead, there is an actual "jamming temperature"  $T_{\rm J}$  that determines the direction  $(-\sin\theta,\cos\theta)$  in the  $\log - \log$  plot of Fig. 4 along the jamming equation of state (see Fig. 13). By maximizing the entropy along this direction we obtain  $T_{\rm J}$  as a function of A and X (see Materials and Methods Section III E):

$$T_{\rm J} = \sin \theta \frac{A}{\Gamma} = \frac{a}{\sqrt{1+a^2}} \frac{A}{\Gamma} \sim (\phi - \phi_c)^{\gamma - a}.$$
 (10)

By the definition of "heat" capacity, we obtain two jamming capacities as the response to changes in A and X:

$$C_{\Gamma} \equiv \partial \Gamma / \partial A \sim (\phi - \phi_c)^{-1} \sim A^{-2/5}$$
, and  $C_{\rm V} \equiv \partial V / \partial X \sim (\phi - \phi_c)^{-1} \sim |X|^{-1/2}$ . (11)

From Eq. (11), the jamming capacities diverge at the jamming transition as  $A \to 0^+$  and  $X \to 0^-$ . However, this result does not imply that the transition is critical since from Einstein fluctuation theory applied to pressure and volume [27] we obtain (we consider  $k_B = 1$  for simplicity):

$$\langle (\Delta \Gamma)^2 \rangle = A^2 C_{\Gamma} \sim A^{1.6}, \text{ and } \langle (\Delta V)^2 \rangle = X^2 C_{V} \sim |X|^{1.5}.$$
 (12)

Thus, the pressure and volume fluctuations near the jamming transition do not diverge, but instead vanish as  $A \to 0^+$  and  $X \to 0^-$ . From a thermodynamical point of view, the transition is not of second order due to the lack of critical fluctuations. As a consequence, no diverging static correlation length can be found at the jamming point during isotropic compression. However, other correlation lengths of dynamic origin may still exist in the response of the jammed system to perturbations, such as those imposed by a shear strain or in vibrating modes [7, 28]. Such a dynamic correlation length would not appear in a purely thermodynamic static treatment as developed here. We note though that responses to shear can be treated in the present formalism by allowing the inverse angoricity to be tensorial [10]. The intensive jamming temperature Eq. (10) gives use to a jamming effective energy  $E_{\rm J}$  as the extensive variable satisfying  $T_{\rm J} = \partial E_{\rm J}/\partial S$  and a full jamming capacity

 $C_{\rm J} \sim (\phi - \phi_c)^{-1}$ , which also diverges at jamming (see Materials and Methods Section III E). However, the fluctuations of  $E_{\rm J}$  defined as  $\langle (\Delta E_{\rm J})^2 \rangle = T_{\rm J}^2 C_{\rm J} \sim T_{\rm J}$  has the same behavior as the fluctuations of volume and pressure, vanishing at the jamming transition  $T_{\rm J} \to 0^+$  [ $A \to 0^+$  in Eq. (10)].

## II. CONCLUSIONS

We have suggested that the concept of "thermalization" at a compactivity and angoricity in jammed systems is reasonable by the direct test of ergodicity. The numerical results indicate that the full canonical ensemble of pressure and volume describes the observables near the jamming transition quite well. From a static thermodynamic viewpoint, the jamming phase transition does not present critical fluctuations characteristic of second-order transitions since the fluctuations of several observables vanish approaching jamming. The lack of critical fluctuations is respect to the angoricity and compactivity under isotropic compression in the jammed phase  $\phi \to \phi_c^+$ , which does not preclude the existence of critical fluctuations when accounting for the full range of fluctuations in the liquid to the jammed phase transition from below  $\phi_c$ . Thus, a critical diverging length scale might still appear as  $\phi \to \phi_c^-$  [29, 30]. Our results suggest an ensemble treatment of the jamming transition. One possible analytical route to use this formalism would be to incorporate the coupling between volume and coordination number at the particle level found in [16] together with similar dependence for the stress to solve the partition function at the mean field level. This treatment would allow analytical solutions for the observables with the goal of characterizing the scaling law near the jamming transition.

### III. MATERIALS AND METHODS

## A. System Information

The systems used for both, ensemble generation and molecular dynamic simulation, are the same. They are composed of 30 spherical particles in a periodic boundary box. The particles have same radius  $r = 5\mu m$  and interact via a Hertz normal repulsive force without

friction. The interaction is defined as:

$$F_n = \frac{2}{3} k_n r^{1/2} (\delta r)^{\delta}, \tag{13}$$

where  $\delta r = (1/2)[2r - |\vec{x}_1 - \vec{x}_2|] > 0$  is the normal overlap and  $k_n = 4G/(1 - \nu)$  is defined in terms of the shear modulus G and the Poisson's ratio  $\nu$  of the material from which the grains are made and  $\delta = 3/2$ . Here, we use G = 29 GPa and  $\nu = 0.2$  for spherical particles and the density of the particles,  $\rho = 2 \times 10^3$  kg/m<sup>3</sup>.

#### B. Ensemble Generation

In this section, we first explain the method to obtain geometrically distinct minima in the PEL. Then we show that the density of the states,  $g(\Gamma, \phi)$ , does not change significantly after sufficient searching time for the configurations.

For N structureless particles possessing no internal orientational and vibrational degrees of freedom, at a fixed volume fraction  $\phi$ , the potential energy is a 3N-dimensional function,  $E(r_1, \ldots, r_N)$ , depending on the positions  $r_i$  of the N particles. In principle, if all local minima corresponding to the mechanically stable configurations of the PEL are obtained, the density of states  $g(\Gamma, \phi)$  can be calculated. Such an exhaustive enumeration of all the jammed states requires that N not be too large due to computational limits. On the other hand, in order to obtain a precise average pressure in the MD simulation,  $\langle p \rangle_{\rm dyn}$ , N cannot be too small such that boundary effects are minimized. Considering these constraints, we choose a 30 particle system.

In order to enumerate all the jammed states at a given volume fraction  $\phi$ , we start by generating initial unjammed packings (not mechanically stable) performing a Monte Carlo (MC) simulation at a high, fixed temperature. The MC part of the method applied to the initial packings assumes a flat exploration of the whole PEL. Every MC unjammed configuration is in the basin of attraction of a jammed state which is defined as a local minimum in the PES with a positive definite Hessian matrix, that is a zero-order saddle. In order to find such a minimum, we apply the LBFGS algorithm provided by Nocedal and Liu [22]. The procedure is analogous to finding the inherent structures [23] of glassy systems. The LBFGS algorithm is also similar to the conjugate gradient method employed by O'Hern et al. [4, 11], but it is computationally more efficient since it does not require

the calculation of the Hessian matrix of the system at any time step. The PEL for each fixed  $\phi$  likely includes millions of geometrically distinct minima by our simulation results. Therefore, an exhaustive search of configurations is computationally long. We check that the number of found configurations has saturated after sufficient trials such that the density of states  $g(\Gamma, \phi)$  has converged to a final shape.

It is also important to determine if the local minima are distinct. Usually, the eigenvalues of the Hessian matrix at each local minimum can be used to distinguish these mechanically stable packings. Here, we follow this idea to compare minima to filter the symmetric packings. However, instead of calculating the eigenvalues of each packing, which is very time consuming, we calculate a function of the distance between any two particles in the packing to improve search efficiency (for the LBFGS algorithm, we do not need to calculate the Hessian matrix). For each packing, we assign the function  $Q_i$  for each particle in the system:

$$Q_i = \sum_{1 \le j \le N, \ j \ne i} \tan^2(\frac{\pi r_{ij}^2}{3L^2}),\tag{14}$$

where  $r_{ij}$  is the distance between particles i and j, L is the system size and N=30 is the number of the particles of the system. We list the  $Q_i$  for each packing from minimum to maximum  $\{Q_i\}(1 \leq i \leq N)$ . Since  $Q_i$  is a higher order nonlinear function, we can assume that two packings are the same if they have the same list. The tolerance is defined as:

$$T = \sqrt{\frac{\sum_{1 \le i \le N} (Q_i - Q_i')^2}{N^2}},$$
(15)

where  $Q_i$  and  $Q_i'$  are the corresponding values from the lists of two packings.

Figure 5 shows the distributions of the tolerance T for packings at different volume fractions. This figure suggests that two packings can be considered the same if  $T \leq 10^{-1}$ , which defines the noise level.

From Fig. 6, we see that after one week of searching,  $g(\Gamma, \phi)$  does not change significantly, since the initial packings are generated by a completely random protocol. We also check the probability (defined as  $\frac{N_{\text{new}}(i)}{N_{\text{total}}(i)}$ , where  $N_{\text{new}}(i)$  is the number of new configurations found on the *i*th day and  $N_{\text{total}}(i)$  is the total number of configurations found in *i* days) of finding new mechanically stable states for different searching days. From Fig. 7, we see that, after one week searching, the probability of finding new configurations at different volume fractions converges, suggesting that enough ensemble packings have been obtained to capture the features of  $g(\Gamma, \phi)$ . A further test of convergence is obtained below in Fig. 11.

#### C. MD Generation

In order to analyze numerical results, we perform MD simulations to obtain  $Z_{\rm dyn}$ ,  $p_{\rm dyn}$  and  $\phi_{\rm dyn}$ , which are herein considered real dynamics. The algorithm is described in detail in [6, 16, 24]. Here, a general description is given: A gas of non-interacting particles at an initial volume fraction is generated in a periodically repeated cubic box. Then, an extremely slow isotropic compression is applied to the system. The compression rate is  $\Gamma_0 = 5.9t_0^{-1}$ , where the time is in units of  $t_0 = R\sqrt{\rho/G}$ . After obtaining a state for which the pressure p is a slightly higher than the prefixed pressure we choose, the compression is stopped and the system is allowed to relax to mechanical equilibrium following Newton's equations. Then the system is compressed and relaxed repeatedly until the system can be mechanically stable at the predetermined pressure. To obtain the statistical average of  $Z_{\rm dyn}$  and  $\phi_{\rm dyn}$ , we repeat the simulation to get enough packing samples having statistically independent random initial particle positions. Here, 250 independent packings are obtained for each fixed pressure (see Fig. 8).

#### D. Angoricity Calculation

Since we obtain  $g(\Gamma, \phi)$  and  $\langle p \rangle_{\text{dyn}}$  for each volume fraction  $\phi$ , we can calculate the inverse angoricity  $\alpha$  by Eq. (1). The pressure  $\langle p(\alpha, \phi) \rangle_{\text{ens}}$  for a given  $\phi$  is a function depending on  $\alpha$  as:

$$\langle p(\alpha, \phi) \rangle_{\text{ens}} = \frac{\int_0^\infty pg(\Gamma, \phi)e^{-\alpha\Gamma} d\Gamma}{\int_0^\infty g(\Gamma, \phi)e^{-\alpha\Gamma} d\Gamma} = \frac{\sum pe^{-\alpha\Gamma}}{\sum e^{-\alpha\Gamma}}.$$
 (16)

Figure 9 shows the result of the numerical integration of Eq. (16) for a particular  $\phi = 0.614$  as a function of  $\alpha$  using the numerically obtained  $g(\Gamma, \phi)$  from Fig. 1. To obtain the value of  $\alpha$  for this  $\phi$ , we input the corresponding measure of the pressure obtained dynamically  $\langle p(\phi) \rangle_{\rm dyn}$  and obtain the value of  $\alpha$  as schematically depicted in Fig. 9. The same procedure is followed for every  $\phi$  (see Fig. 10) and the dependence  $\alpha(\phi)$  is obtained. The result is shown in Fig. 2B in the main text.

We also check the inverse angoricity  $\alpha(\phi)$  using  $g(\Gamma, \phi)$  for different searching days (see Fig. 6) to ensure the accuracy and convergence to the proper value. From Fig. 11, we can see that, after 10 days searching,  $\alpha(\phi)$  is stable due to the fact that the density of state,

 $g(\Gamma, \phi)$ , does not change significantly. For volume fraction much larger than  $\phi_c$ , the system's input pressure  $\langle p(\phi)\rangle_{\rm dyn}$  reaches the plateau at low  $\alpha$  of the function  $\langle p(\alpha, \phi)\rangle_{\rm ens}$  (see Fig. 10) and the corresponding  $\alpha(\phi)$  becomes much smaller (the angoricity  $A(\phi)$  becomes much larger), leading to large errors in the value of A as  $\phi$  becomes large. This might explain the plateau found in A when  $(\phi - \phi_c) > 2 \times 10^{-2}$  as shown in Fig. 2B.

Using  $\alpha(\phi)$  for each volume fraction, we calculate  $\langle Z \rangle_{\text{ens}}$  by:

$$\langle Z(\phi) \rangle_{\text{ens}} = \frac{\int_0^\infty Zg(\Gamma, \phi) e^{-\alpha\Gamma} d\Gamma}{\int_0^\infty g(\Gamma, \phi) e^{-\alpha\Gamma} d\Gamma} = \frac{\sum Ze^{-\alpha\Gamma}}{\sum e^{-\alpha\Gamma}},$$
(17)

the average force  $\langle \overline{F} \rangle_{\text{ens}}$  by:

$$\langle \overline{F}(\phi) \rangle_{\text{ens}} = \frac{\int_0^\infty \overline{F} g(\Gamma, \phi) e^{-\alpha \Gamma} d\Gamma}{\int_0^\infty g(\Gamma, \phi) e^{-\alpha \Gamma} d\Gamma} = \frac{\sum \overline{F} e^{-\alpha \Gamma}}{\sum e^{-\alpha \Gamma}},$$
(18)

where  $\overline{F}$  is the average force for each ensemble packing and the force distribution  $P_{\text{ens}}(F/\overline{F})$  by:

$$P_{\rm ens}(F/\overline{F}) = \frac{\int_0^\infty P(F/\overline{F})g(\Gamma,\phi)e^{-\alpha\Gamma}d\Gamma}{\int_0^\infty g(\Gamma,\phi)e^{-\alpha\Gamma}d\Gamma} = \frac{\sum P(F/\overline{F})e^{-\alpha\Gamma}}{\sum e^{-\alpha\Gamma}}.$$
 (19)

Equations (17)–(19) are then compared with the dynamical measures for a test of ergodicity in Fig. 3 in the main text.

#### E. Entropy Calculation

Here we present the calculation of the "jamming temperature"  $T_{\rm J}$  and the corresponding jamming "heat" capacity  $C_{\rm J}$ . From the power-law relation  $p = \Gamma/V \propto (\phi - \phi_c)^a$ , we have:

$$ln p = ln p_0 + a ln(\phi - \phi_c),$$
(20)

where  $p_0$  is the constant depending on the system and the slope  $\tan \theta = a$ . Figure 4 indicates that the jammed system always remain at the positions of maximal entropy  $\delta S = 0$  in the direction  $(-\sin \theta, \cos \theta)$ , perpendicular to the jamming power-law curve. In order to further analyze this result, we plot the entropy distribution along the direction  $(-\sin \theta, \cos \theta)$  in Fig. 12. We see that the entropy of the corresponding jammed states remains at the peak of the distributions along  $(-\sin \theta, \cos \theta)$ , verifying the maximum entropy principle in this particular direction. We notice that some deviations are found in the vicinity of  $\phi_c$ . The maximization of entropy is not on  $\Gamma$  or V alone, but on a combination of both. This means

that the entropy  $S(\ln(\langle \phi \rangle_{\text{dyn}} - \phi_c), \ln \langle p \rangle_{\text{dyn}})$  is maximum along the direction of  $(-\sin \theta, \cos \theta)$  and the slope of the entropy along this direction  $(-\sin \theta, \cos \theta)$  is 0 (see Fig. 13), that is,

$$\frac{\partial S}{\partial \ln(\phi - \phi_c)} \sin \theta = \frac{\partial S}{\partial \ln p} \cos \theta. \tag{21}$$

Thus we verify the second law of thermodynamics for jammed systems:  $\delta S = 0$  at  $(\ln(\langle \phi \rangle_{\rm dyn} - \phi_c), \ln \langle p \rangle_{\rm dyn})$ .

By the definition of angoricity  $A = \partial \Gamma / \partial S$  and compactivity  $X = \partial V / \partial S$ , we have:

$$\frac{\partial S}{\partial \ln p} = p \frac{\partial S}{\partial p} = \Gamma \frac{\partial S}{\partial \Gamma} = \frac{\Gamma}{A} = \frac{c_1}{A},\tag{22}$$

$$\frac{\partial S}{\partial \ln(\phi - \phi_c)} = (\phi - \phi_c) \frac{\partial S}{\partial \phi} = (\phi - \phi_c) \frac{\partial V}{\partial \phi} \frac{1}{X} = -(\phi - \phi_c) \frac{NV_g}{\phi^2} \frac{1}{X} = -\frac{c_2}{X}, \tag{23}$$

where  $\phi = NV_g/V$ ,  $c_1 = \Gamma$  and  $c_2 = (\phi - \phi_c)(NV_g/\phi^2)$ . By Eq. (22) and Eq. (23), we can simplify Eq. (21):

$$\frac{c_1}{A} + a\frac{c_2}{X} = 0. (24)$$

The relation between X and A can be obtained then:

$$X = -a\frac{c_2}{c_1}A = -a\frac{\phi - \phi_c}{p\phi}A. \tag{25}$$

Since we obtain the angoricity  $A \propto (\phi - \phi_c)^{\gamma}$  with  $\gamma = 2.5$  in the main text and the pressure  $p \propto (\phi - \phi_c)^a$  with a = 1.5 (actually we get 1.65 for the small system size used in the main text but the difference can be neglected to simplify). The compactivity  $X \propto -(\phi - \phi_c)^2/\phi$ . We can therefore define the "jamming temperature"  $T_J$  as a function of the slope along the direction  $(\cos \theta, \sin \theta)$ :

$$\frac{1}{T_{\rm J}} = \frac{c_1}{A}\sin\theta - \frac{c_2}{X}\cos\theta = \cos\theta \left(a\frac{c_1}{A} - \frac{c_2}{X}\right) = \frac{c_1}{A\sin\theta} = -\frac{c_2}{X\cos\theta}.$$
 (26)

That is:

$$T_{\rm J} = \frac{A\sin\theta}{c_1} = -\frac{X\cos\theta}{c_2} = \frac{\sin\theta}{\Gamma}A = \frac{a}{\sqrt{1+a^2}}\frac{A}{\Gamma} \sim (\phi - \phi_c)^{\gamma - a} \sim (\phi - \phi_c). \tag{27}$$

Furthermore, the "jamming energy"  $E_{\rm J}$ , corresponding to the "jamming temperature"  $T_{\rm J}$ 

in Eq. (27), has the relation as below:

$$dE_{J} = T_{J}dS$$

$$= T_{J}\frac{\partial S}{\partial \ln(\phi - \phi_{c})}d\ln(\phi - \phi_{c}) + T_{J}\frac{\partial S}{\partial \ln p}d\ln p$$

$$= (-\frac{X\cos\theta}{c_{2}})(-\frac{c_{2}}{X})d\ln(\phi - \phi_{c}) + \frac{A\sin\theta}{c_{1}}\frac{c_{1}}{A}d\ln p$$

$$= \cos\theta d\ln(\phi - \phi_{c}) + \sin\theta d\ln p$$

$$= (\cos\theta + \sin\theta \tan\theta)d\ln(\phi - \phi_{c})$$

$$= \frac{d\ln(\phi - \phi_{c})}{\cos\theta}.$$
(28)

That is,

$$dE_{\rm J} = \sqrt{a^2 + 1} d\ln(\phi - \phi_c), \tag{29}$$

and

$$E_{\rm J} = (\sqrt{a^2 + 1}) \ln(\phi - \phi_c).$$
 (30)

The jamming capacity  $C_{\rm J}$  can be obtained as:

$$C_{\rm J} = T_{\rm J} \frac{\partial S}{\partial T_{\rm J}} = T_{\rm J} \frac{\partial S}{\partial \ln p} \frac{\partial \ln p}{\partial T_{\rm J}} + T_{\rm J} \frac{\partial S}{\partial \ln(\phi - \phi_c)} \frac{\partial \ln(\phi - \phi_c)}{\partial T_{\rm J}}, \tag{31}$$

Finally, with Eq. (21)–(23), the capacity  $C_{\rm J}$  can be calculated:

$$C_{\rm J} = T_{\rm J} \left(\frac{c_1}{A} - \frac{c_2}{aX}\right) \frac{\partial \ln p}{\partial T_{\rm J}} = T_{\rm J} \frac{1 + a^2}{a^2} \frac{c_1}{A} \frac{\partial \ln p}{\partial T_{\rm J}}.$$
 (32)

Since  $T_{\rm J} \sim (\phi - \phi_c)$  and  $p \sim (\phi - \phi_c)^{1.5}$ , we obtain  $C_{\rm J} \sim (\phi - \phi_c)^{-1}$ .

- [1] Coniglio, A., Fierro, A., Herrmann, H. J. & Nicodemi, M. Unifying Concepts in Granular Media and Glasses (Elsevier, Amsterdam, 2004).
- [2] Behringer, R. P. & Jenkins, J. T. Powders and Grains Vol. 97 (Balkema, Rotterdam, 1997).
- [3] Liu, A. J. & Nagel, S. R. Jamming is not just cool anymore. *Nature* **396**, 21-22 (1998).
- [4] O'Hern, C. S., Langer, S. A., Liu, A. J. & Nagel, S. R. Random packings of frictionless particles. *Phys. Rev. Lett.* 88, 075507-075510 (2002).
- [5] Makse, H. A., Johnson, D. & Schwartz, L. Packing of compressible granular materials. Phys. Rev. Lett. 84, 4160-4163 (2000).
- [6] Makse, H. A., Gland, N., Johnson, D. L. & Schwartz, L. M. Granular packings: nonlinear elasticity, sound propagation, and collective relaxation dynamics. *Phys. Rev. E* 70, 061302 (2004).
- [7] Ellenbroek, W. G., Somfai, E., van Hecke, M & van Saarloos, W. Critical scaling in linear response of frictionless granular packings near jamming. *Phys. Rev. Lett.* **97**, 258001 (2006).
- [8] Henkes, S. & Chakraborty, B. Jamming as a critical phenomenon: a field theory of zero-temperature grain packings. *Phys. Rev. Lett.* **95**, 198002 (2005).
- [9] Henkes, S., O'Hern, C. S. & Chakraborty, B. Entropy and temperature of a static granular assembly: an *ab initio* approach. *Phys. Rev. Lett.* **99**, 038002 (2007).
- [10] Henkes, S. & Chakraborty, B. Statistical mechanics framework for static granular matter. Phys. Rev. E 79, 061301 (2009).
- [11] Xu, N., Blawzdziewicz, J. & O'Hern, C. S. Random close packing revisited: how many ways can we pack frictionless disks? *Phys. Rev. E* **71**, 061306 (2005).
- [12] Edwards, S. F. The role of entropy in the specification of a powder, in *Granular matter: an interdisciplinary approach* (ed, Mehta, A.) (Springer-Verlag, New York, 1994).
- [13] Edwards, S. F. The full canonical ensemble of a granular system. *Physica A* **353**, 114-118 (2005).
- [14] Edwards, S. F. & Grinev, D. V. Statistical mechanics of stress transmission in disordered granular arrays. *Phys. Rev. Lett* **82**, 5397-5400 (1999).
- [15] Ball, R. C. & Blumenfeld, R. Stress field in granular systems: loop forces and potential formulation. *Phys. Rev. Lett.* **88**, 115505 (2002).

- [16] Song, C., Wang, P. & Makse, H. A. A phase diagram for jammed matter. *Nature* 453, 629-632 (2008).
- [17] Brujić, J., Edwards, S. F., Hopkinson, I. & Makse, H. A. Measuring distribution of interdroplet forces in a compressed emulsion system. *Physica A* **327**, 201-212 (2003).
- [18] Goldstein, M. Viscous liquids and the glass transition: a potential energy barrier picture. J. Chem. Phys. 51, 3728-3739 (1969).
- [19] Stillinger, F. H. & Weber, T. A. Hidden structure in liquids. Phys. Rev. A 25, 978-989 (1982).
- [20] Sastry, S., Debenedetti, P.G. & Stillinger F.H. Identification of potential energy landscape signatures of distinct dynamical regimes in a glass forming liquid. *Nature* **393**, 554-557 (1998).
- [21] Landau, L. D. & Lifshitz, E. M. Theory of Elasticity (Pergamon, NY, 1970).
- [22] Liu, D. C. & Nocedal, J. On the limited memory method for large scale optimization. *Mathematical Programming B* **45**, 503-528 (1989).
- [23] Doye, J. P. K. & Wales, D. J. Saddle points and dynamics of Lennard-Jones clusters, solids, and supercooled liquids. J. Chem. Phys. 116, 3777-3788 (1994).
- [24] Zhang, H. P. & Makse, H. A. Jamming transition in emulsions and granular materials. *Phys. Rev. E* **72**, 011301 (2005).
- [25] O'Hern, C. S., Langer, S. A., Liu, A. J. & Nagel, S. R. Force distributions near jamming and glass transitions. *Phys. Rev. Lett.* **86**, 111-114 (2001).
- [26] Snoeijer, J. H., Vlugt, T. J. H., van Hecke, M. & van Saarloos, W. Force network ensemble: a new approach to static granular matter. *Phys. Rev. Lett.* **92**, 054302 (2004).
- [27] Landau, L. D. & Lifshitz, E. M. Statistical Physics (Pergamon, New York, 3rd edition 1980).
- [28] Wyart, M., Nagel, S. R. & Witten T. A. Geometric origin of excess low-frequency vibrational modes in weakly connected amorphous solids. *Europhys. Lett.* 72, 486-492 (2005).
- [29] Ciamarra, M. P. & Coniglio, A. Jamming at zero temperature, zero friction, and finite applied shear stress. Preprint at \( \text{http://arxiv.org/abs/0907.1605} \) (2009).
- [30] Dauchot, O., Marty, G. & Biroli, G. Dynamical heterogeneity close to the jamming transition in a sheared granular material. *Phys. Rev. Lett.* **95**, 265701 (2005).

- Fig. 1. Ensemble calculations. The density of states  $g(\Gamma, \phi)$  as a function of internal virial  $\Gamma$  for different volume fraction,  $\phi$ , ranging from 0.610 to 0.670. The inset is a schematic two-dimensional potential energy landscape surface. The jammed states A and B are local minima (zero order saddles) in the PES where the external force for each particle is zero and the Hessian matrix of the system is positive definite. Our simulation system consists of 30 frictionless spherical particles interacting by Hertzian forces with periodic boundary conditions.
- Fig. 2. Scaling of pressure and inverse angoricity. (A) The blue  $\bigcirc$  shows the power-law relation for  $\langle p \rangle_{\rm dyn}$  vs  $\langle \phi \rangle_{\rm dyn} \phi_c$  for the 30-particle system. Here, the pressure  $\langle p \rangle_{\rm dyn}$  are average values obtained by 250 independent MD simulations. The red  $\bigcirc$  is the pressure used to obtain the inverse angoricity  $\alpha$  predicted by Eq. (4). The relatively small system size results in large fluctuations of the observables. In order to predict a precise relation for the system (N=30), sufficient independent samples of the packings are generated to calculate the precise average for observables. We prepare 250 independent packings for each  $\phi$  to get enough statistical samples to obtain  $\langle p \rangle_{\rm dyn}$  and  $\langle Z \rangle_{\rm dyn}$  by statistical average (see Fig. 8). The inset shows a semi-log plot. (B) The inverse angoricity  $\alpha$  as a function of  $\phi$ - $\phi_c$ . We find a power-law relation for system's volume fraction  $\phi$  near  $\phi_c$ . The solid line has a slope of -2.5. The inset is the angoricity  $A(=1/\alpha)$  vs  $\phi$ - $\phi_c$ . The plateau observed in A for large volume fraction  $\phi$  might be related to the finite size of the sample.
- Fig. 3. Test of ergodicity. (A) The blue  $\bigcirc$  is the average coordination number  $\langle Z \rangle_{\rm dyn}$  obtained by 250 independent MD simulations. The red  $\bigcirc$  is the coordination number  $\langle Z \rangle_{\rm ens}$  calculated by the ensemble for different volume fractions. Agreement between both measures supports the concept of ergodicity in the system. (B) The same as (A) but in a log-log plot. The blue  $\bigcirc$  shows the power-law relations for  $\langle Z \rangle_{\rm dyn}$ - $Z_c$  vs  $\langle \phi \rangle_{\rm dyn}$ - $\phi_c$  for 30-particle system with  $\phi_c = 0.6077$  and  $Z_c = 5.82$ . (C) Comparison of  $\langle \overline{F} \rangle_{\rm dyn}$  and  $\langle \overline{F} \rangle_{\rm ens}$  for different volume fractions. (D) The comparison of selected distributions of forces  $P_{\rm dyn}(F/\overline{F})$  and  $P_{\rm ens}(F/\overline{F})$  for different volume fractions.
- Fig. 4. Microcanonical calculations. The entropy surface  $S(\ln(\phi \phi_c), \ln p)$ . The color bar indicates the value of the entropy. The superimposed blue  $\bigcirc$  is  $\langle p(\phi) \rangle_{\rm dyn}$  from MD calculations as in Fig. 2a. The olive arrow line indicates the maximization direction of the entropy  $(-\sin\theta, \cos\theta)$ . Following this direction, the entropy is maximum at the point  $(\ln(\langle \phi \rangle_{\rm dyn} \phi_c), \ln \langle p \rangle_{\rm dyn})$ , corroborating the maximum entropy principle.

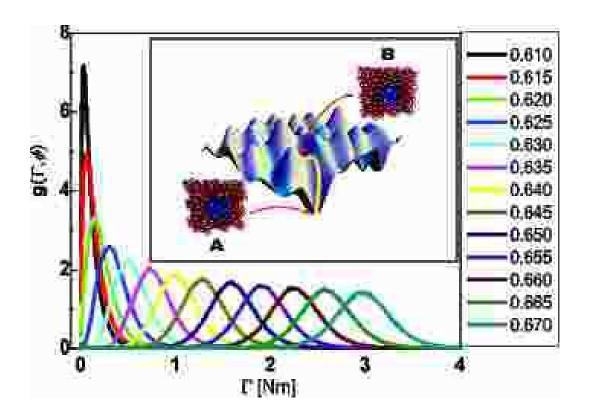


FIG. 1:

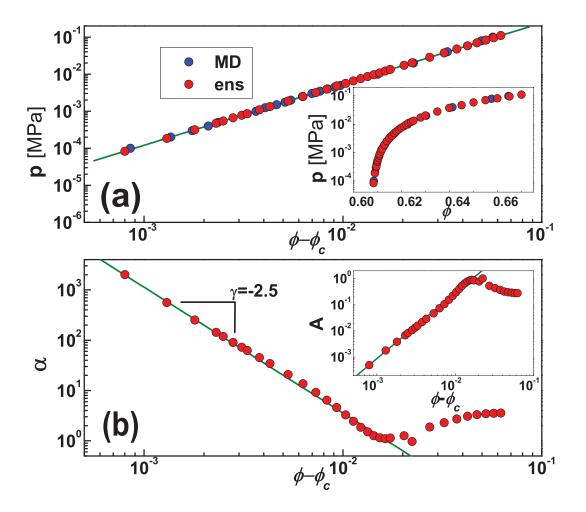


FIG. 2:

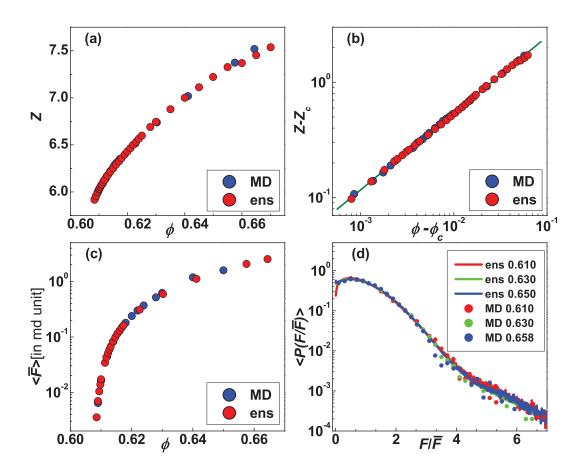


FIG. 3:

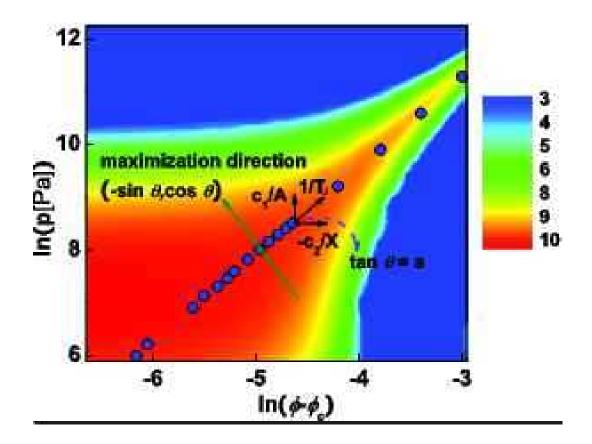


FIG. 4:

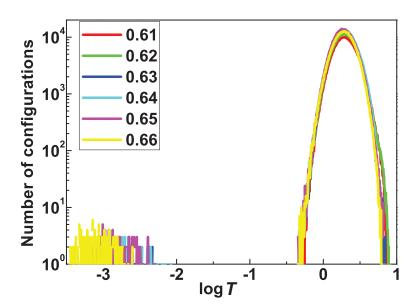


FIG. 5: The distribution of the tolerance T between any two packings at the given  $\phi$ . From the graph, the value of T for which any two different packings are considered to be same is chosen to be  $10^{-1}$ , which is above the noise threshold and below the distribution of T.

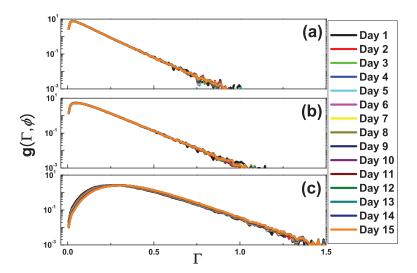


FIG. 6: The distribution of  $g(\Gamma, \phi)$  for 15 days searching (A) at  $\phi = 0.609$ , (B) at  $\phi = 0.614$ , (C) at  $\phi = 0.625$ . Different color in (A), (B), (C) corresponds to the different day. We find that after 15 days the distributions have converged.

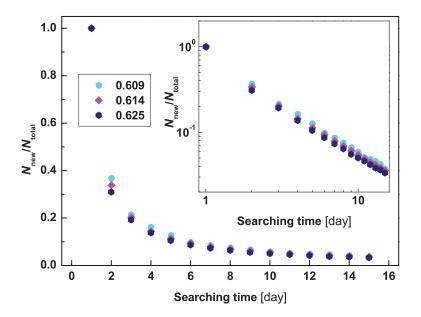


FIG. 7: The probability to find new configurations for different searching day.

FIG. 8: The cyan  $\bigcirc$  is  $Z_{\rm dyn}$  and  $\phi_{\rm dyn}$  for every single packing obtained with MD and the blue  $\bigcirc$  are the average over the single packings for the system which are then shown in the main text of the paper.

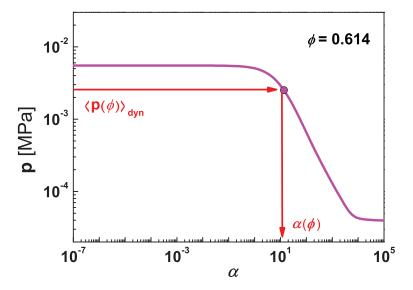


FIG. 9: The numerical integration of Eq. (16) for  $\phi = 0.614$  is shown as the pink curve. We input the  $\langle p \rangle_{\rm dyn}$  (pink  $\bigcirc$  in the plot) and obtain the corresponding inverse angoricity  $\alpha$ .

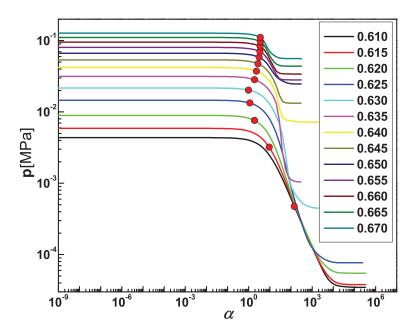


FIG. 10: Calculation of  $\alpha$  for several volume fractions  $\phi$  as explained in detail in Fig. 9

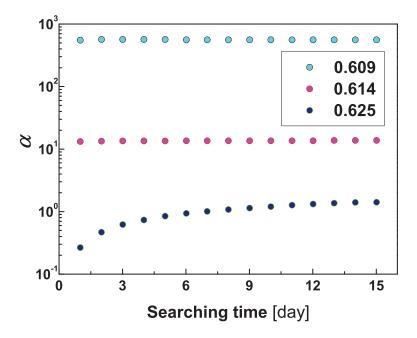


FIG. 11: Calculation of inverse angoricity  $\alpha$  for different searching day.

FIG. 12: The distribution of entropy  $S(\ln p, \ln(\phi - \phi_c))$  along the direction  $(-\sin \theta, \cos \theta)$  for different jamming ensemble points. The blue  $\bigcirc$  are the entropy for jammed system, which is the maximum of S, verifying the second law of thermodynamics. We notice that some deviations are found near  $\phi_c$ .

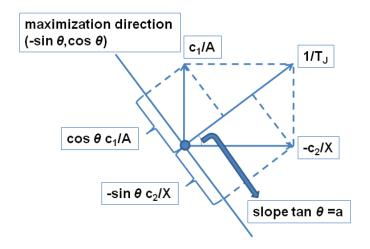


FIG. 13: The representation of the maximization analysis  $\delta S = 0$  along the direction  $(-\sin\theta,\cos\theta)$  for one point in the jamming power-law curve. Here  $c_1 = \Gamma$  and  $c_2 = (\phi - \phi_c)(NV_g/\phi^2)$ .